EXTREME VALUE ANALYSIS OF COASTAL INUNDATION FOR THE DESIGN OF COASTAL PROTECTION IN CAMARINES SUR, PHILIPPINES

Elias A. Garcia[1], Eric C. Cruz[2,3], Vince Rainer A. Abrigonda[1], and Andrei Raphael P. Dita[1]

Coastal flooding is a natural hazard that is eminent in many Philippine coastlines. Both storm tide flooding and wave overtopping have been found to occur along Philippine coastlines and they usually also cause coastal erosion in coastlines where there is no natural protection against the waves and tides. To appropriately design coastal protection structures to mitigate these hazards, ensuring sufficient level of protection and considering economic constraints (i.e., cost), it is necessary to determine the design water level among other parameters. For design purposes, it is important to know the frequency of occurrence of extreme water levels. However, there are no long-term water level records in the project area, so an alternative approach via extreme value analysis was performed based on simulated water levels from numerical simulations. The resulting coastal inundation corresponding to 100-yr return period, the level of protection required for urban areas as per DPWH DGCS Volume 3, ranges from 0.38 to 2.34 m along the project coastline while for urban areas with 25-yr return period, the design coastal inundation reaches up to 1.65 m. Coastal protection structures to be proposed should then be vertically sited higher than these design water levels.

Keywords: disaster mitigation; numerical simulation; extreme value analysis; typhoon; coastal protection

INTRODUCTION

Coastal flooding is a natural hazard that is eminent in many Philippine coastlines as the region is frequented by typhoons annually. It results when the storm tide level exceeds the inland topography and inundates it over a sustained duration (Fig. 1).

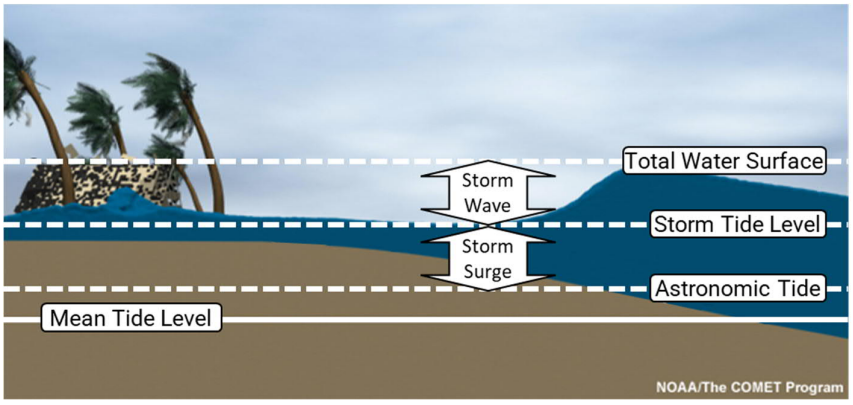

Figure 1. Illustration of tide and wave components during a typhoon (National Oceanic and Atmospheric Administration, 2019).

Coastal flooding also results when sea waves overtop the backshore and cyclically bring large volumes of seawater that spread over the backshore in a recursive manner, although the storm tide level is lower than the backshore elevation. The former mode of coastal flooding is storm tide flooding, and the second is wave overtopping. Both storm tide flooding and wave overtopping have been found to occur along Philippine coastlines and they usually also cause coastal erosion in coastlines where there is no natural protection against the waves and tides.

Coastal erosion along the shorelines of Camarines Sur (Fig. 2) has been raised as an issue affecting the infrastructure and population within the area. Analysis of the wave overtopping on seawalls will also provide useful information on the overtopping duration for purposes of infrastructure rehabilitation and/or disaster evacuation planning (Rizabal and Cruz, 2020). A simulative analysis of the more serious case of coastal inundation resulting from the overtopping of the backshore or of the seawall by storm tides will determine the inland extent of the inundation (Camelo et al., 2017)

[1] AMH Philippines, Inc., Ang Bahay ng Alumni Building, University of the Philippines-Diliman, Quezon City, 1101, Philippines
[2] UP National Engineering Center, University of the Philippines-Diliman, Quezon City, 1101, Philippines
[3] Institute of Civil Engineering, University of the Philippines-Diliman, Quezon City, 1101, Philippines

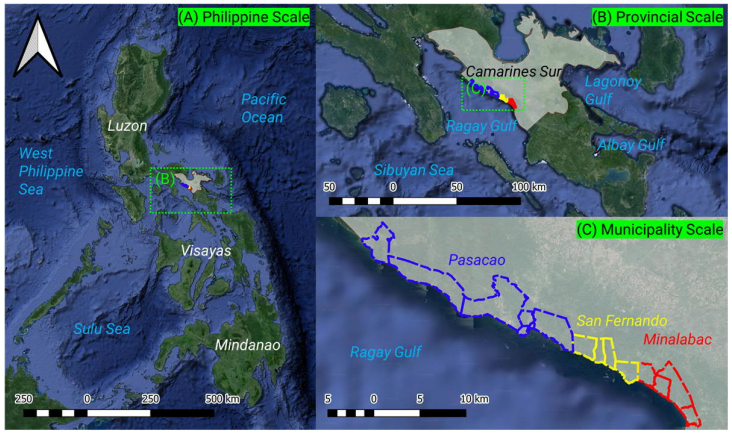

Figure 2. Project location – Camarines Sur.

To address these issues, baseline and advanced coastal engineering studies were carried out, concentrating on assessing a proposed seawall alignment along the Camarines Sur coastline. The primary objective of the seawall was to safeguard inland developments from coastal hazards and reduce the impact of coastal erosion.

The coastline of interest lies completely along the northeastern boundary of Ragay Gulf, an elongated water body, with the south-eastern terminus in Jamuraon Bay. The project study area stretches along the coastal municipalities of Camarines Sur, covering approximately 45.8km of shoreline (Fig. 3) including Pasacao to the west, Minalabac to the east, and San Fernando in the middle. Along this stretch of shoreline, 18 different sections have already been identified by DPWH as potential alignments for the seawall, totaling approximately 29.5km (Department of Public Works and Highways, 2018) (Fig. 4).

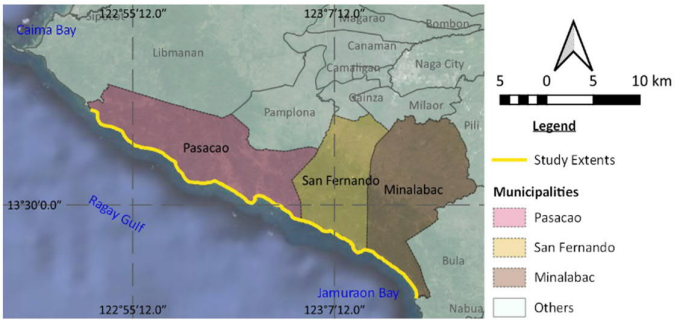

Figure 3. Project coastline and nearby municipalities.

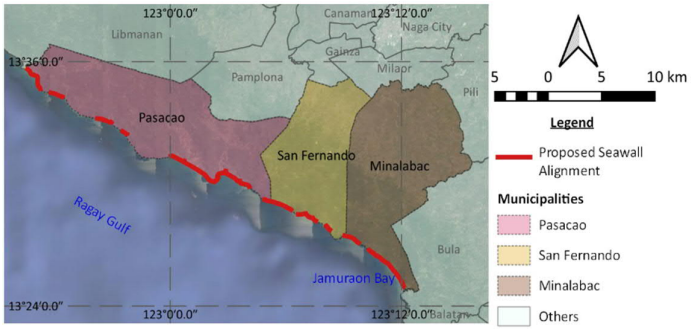

Figure 4. Proposed seawall alignments from the Terms of Reference (Department of Public Works and Highways, 2018).

To appropriately design coastal protection structures, ensuring sufficient level of protection and considering economic constraints (i.e., cost), it is necessary to determine the design water level among other parameters. For design purposes, it is important to know the frequency of occurrence of extreme water levels. However, there are no long-term water level records in the project area, so an alternative approach via extreme value analysis was performed based on simulated water levels from numerical simulations.

The general objective of this paper is to assess extreme coastal inundation along the project coastline using a combined approach of data analysis and numerical modeling, which may also be applicable in obtaining design parameters on non-coastal hazards with limited data. This useful coastal engineering methodology also addresses a persistent and widespread infrastructure planning and design issue for disaster mitigation.

STUDY FLOWCHART

The study can be divided into three major parts: selection of historical tropical cyclones, generation of hydrodynamic (tide) model, and synthesis of coastal inundation (Fig. 5). As the wind is one of the primary forcings that affect the storm tide levels of a passing tropical cyclone, selection of historical tropical cyclones takes precedence. Shortlisting of tropical cyclones was done to filter out the extensive list of typhoons that passed within a search radius from the site and retain those that were deemed critical in terms of wind speed simulated in specified kernels along the project coastline. Atmospheric forcings were modeled via Holland's (1980) single-vortex cyclonic wind model that utilized the meteorological data from Japan Meteorological Agency (JMA) tropical cyclone database.

Given the bathymetry data obtained from secondary sources and tide boundary conditions from a global tide model, the regional mesh was developed, covering the entire Philippine archipelago and surrounding waters. A combined bathymetry-topography local mesh was then developed that consolidates the various available data of water depths and surface topography.

Numerical simulations via MIKE 21 were carried out to synthesize the design basis magnitude of coastal inundation along the project coastline generated by 50 shortlisted historical typhoons from 1951 to 2020. Calibration was conducted by optimizing model parameters such as bed roughness and validation was done using available secondary water levels and coastal inundation data for specific typhoons. Local domain discretization was optimized to yield an acceptable compromise of computational efficiency, model stability, and accuracy since the simulations involve 50 typhoons that each required more than 2 days to complete.

Upon consolidating the coastal inundation output from the 50 historical cyclones, the Annual Maximum Series of simulated coastal inundation at specified kernels were extracted and tested against various probability distributions to determine the best fit distribution. The design coastal inundations were then determined based on the level of protection required of the designated land use of the area.

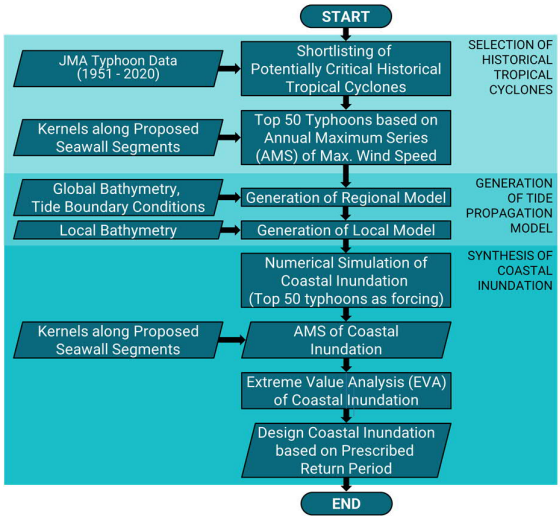

Figure 5. Study flowchart.

TYPHOON SHORTLISTING

A tropical cyclone, characterized by a large low-pressure area is caused by large temperature differences between the sea surface and air temperature above. Typhoons, which are tropical cyclones with sustained wind speeds exceeding about 32m/s (115km/hr), generate strong winds, with the strongest winds centering near the eye of the typhoon. Over deep open waters, these strong sustained winds can generate much higher wave heights than prevailing (i.e., non-storm) winds. The wind speed is one of the primary forcings that affect both storm surge and storm wave of a passing tropical cyclone. A higher velocity wind speed occurring during a tropical cyclone can induce higher storm surges and waves.

Potentially Critical Typhoons

A tropical cyclone, characterized by a large low-pressure area is caused by large temperature differences between the sea surface and air temperature above. Typhoons, which are tropical cyclones with sustained wind speeds exceeding about 32m/s (115km/hr), generate strong winds, with the strongest winds centering near the eye of the typhoon. Over deep open waters, these strong sustained winds can generate much higher wave heights than prevailing (i.e., non-storm) winds. The wind speed is one of the primary forcings that affect both storm surge and storm wave of a passing tropical cyclone. A higher velocity wind speed occurring during a tropical cyclone can induce higher storm surges and waves.

The project coastline has varying coastal morphology and orientation, meaning different wind speeds, and thus storm surge elevations, may be experienced for any given typhoon. To better characterize the different exposures, thirteen (13) data kernels were set along the proposed seawall alignment, considering different coastal morphologies, presence of built-up areas, and presence of river outfalls (Figure 6). The use of wind data kernels for the 45.8-km-long project coastline is an extension of the method applied in Cruz et al. (2016) which is suited to a much shorter 1.35-km built-up coastline.

Figure 6. Wind data kernels along the project coastline.

To determine the annual maximum wind speed caused by a passing tropical cyclone, a long list of tropical cyclones that passed within 250km of the seawall alignment was determined from the JMA database. For years where multiple tropical cyclones occurred, weaker and further storms were further filtered out if it was readily apparent that they would not induce a higher wind speed at any of the kernels. The strength of the tropical cyclone can be estimated by the reported distance from the site and central pressure, i.e., a lower central pressure correlates to a stronger tropical cyclone. For instances when it is difficult to ascertain from the distance and central pressure, more than 1 cyclone was included for further analyses.

This selection and filtering were done for all cyclone data available between 1951 to 2020 from the JMA best track database, resulting in 102 potentially annually critical cyclones that may have induced the maximum cyclonic wind speed along the project shoreline (Table 1).

Table 1. Potentially Critical Typhoons.

Year	Int'l Name	Year	Int'l Name	Year	Int'l Name
1951	Iris	1975	Alice	1997	Mort
1952	Trix	1976	Ruby	1998	Babs
1952	Della	1977	Kim	1999	Eve
1952	Wilma	1978	Lola	2000	Xangsane
1953	Betty	1978	Rita	2001	Lingling
1954	Ruby	1979	Mac	2002	Tapah
1955	Patsy	1979	Vera	2003	Nepartak
1956	Polly	1980	Forrest	2004	Muifa
1956	Thelma	1980	Belly	2004	Nida
1957	Kit	1981	Hazen	2004	Nanmadol
1958	Kathy	1981	Lee	2005	Tembin
1959	Harriet	1981	Irma	2006	Xangsane
1959	Freda	1982	Irving	2006	Durian
1960	Olive	1982	Roger	2007	Hagibis
1960	Kit	1983	Vera	2008	Fengshen
1961	Ellen	1984	Betty	2009	Nangka
1962	Hope	1984	Agnes	2009	Mirinae
1962	Patsy	1985	Dot	2010	Conson
1963	Carmen	1986	Georgia	2011	Nock-Ten
1964	Opal	1987	Nina	2012	Son-Tinh
1964	Winnie	1987	Betty	2013	Rumbia
1965	Patsy	1988	Roy	2013	Nari
1965	Amy	1988	Ruby	2014	Rammasun
1966	Nancy	1989	Dan	2014	Hagupit
1966	Pamela	1989	Hunt	2015	Melor
1967	Emma	1990	Nathan	2016	Nock-Ten
1968	Ora	1991	Yunya	2017	Haikui
1970	Joan	1992	Colleen	2017	Doksuri
1970	Patsy	1993	Lola	2018	Mankut
1971	Dinah	1993	Manny	2018	Usagi
1971	Jean	1994	Teresa	2019	Kammuri
1972	Kit	1994	Axel	2020	Goni
1973	Ruth	1995	Angela	2020	Molave
1974	Ivy	1996	Ann	2020	Vongfong

Cyclonic Wind Field Model

Meteorological parameters of potentially critical typhoons such as central pressure (P_c), maximum wind speed (V_{max}), and radii of 30-kt and 50-kt wind speeds (R_{30} and R_{50}, respectively) were gathered from Japan Meteorological Agency (JMA). The passing distance, defined as the closest distance of the typhoon's center from the project coast, was computed based on the interpolated track data every 6 hours from JMA. These typhoon parameters vary along their tracks as they traverse the Western North Pacific. Hence, a time-dependent, two-dimensional pressure and wind field can be formulated from these parameters.

To determine the two-dimensional (2D) pressure and wind fields from the JMA database, Holland's single vortex model (1980) was applied as the cyclonic model. MIKE 21 cyclone generation toolbox was used to generate the atmospheric wind gradient (V_G) and pressure fields (P). The inputs were the time-dependent central pressure (P_c), ambient pressure (P_n = 1,010 hPa), radius of maximum wind speed (RMW), and the distance from center of the typhoon (r). RMW was computed by fitting the JMA data points for the 30-kt and 50-kt wind speeds and their corresponding radii, to the formula for gradient wind speed (V_G) which utilizes the Holland shape parameter (B), density of air (ρ), and pressure difference (ΔP). Using the time-dependent parameters for each typhoon, the wind and pressure fields were determined. The Holland single vortex model was used to calculate the 2D wind field as given by Eq. (1) while the pressure field is determined from the pressure distribution Eq. (2):

$$V_G(r) = \sqrt{\left(\frac{RMW}{r}\right)^B \frac{B\Delta P \exp\left[-\left(\frac{RMW}{r}\right)^B\right]}{\rho} + \frac{r^2 f^2}{4}} - \frac{rf}{2} \tag{1}$$

$$P(r) = P_c + (P_n + P_c) \cdot \exp\left[-\left(\frac{RMW}{r}\right)^B\right] \tag{2}$$

Annual Maximum Series of Kernel Winds

The generated wind speeds for all tropical cyclones from 1951-2020 across all kernels (Fig. 5) were analyzed, and the Annual Maximum Series (AMS) or the highest wind speed value that occurs within each year was determined.

A sample AMS of top 50 typhoons at KP6 (Pasacao) wind kernel is shown in Table 2 based on decreasing wind speed. The cyclonic models generated the highest wind speed of 53.93 m/s at KP6 which was due to 1987 typhoon Betty (local name: Herming).

Table 2. Sample typhoon wind AMS at KP6 wind kernel.

Rank	Date and Time	Wind Speed (m/s)	Int'l Name	Rank	Date and Time	Wind Speed (m/s)	Int'l Name
1	1987-08-12 13:00	53.93	Betty	26	2004-05-17 1:00	32.84	Nida
2	1970-10-13 7:00	49.81	Joan	27	2000-10-28 1:00	31.64	Xangsane
3	1981-11-23 6:00	49.74	Irma	28	1982-09-08 18:00	30.68	Irving
4	2019-12-02 18:00	49.61	Kammuri	29	1960-10-06 15:00	30.33	Kit
5	2020-11-01 1:00	49.15	Goni	30	2003-11-14 3:00	27.82	Nepartak
6	2016-12-25 18:00	48.40	Nock-Ten	31	2012-10-24 21:00	26.25	Son-Tinh
7	1995-11-02 16:00	48.18	Angela	32	1966-11-19 22:00	25.32	Nancy
8	2006-11-30 7:00	47.79	Durian	33	2009-06-24 1:00	25.22	Nangka
9	2014-07-15 15:00	45.62	Rammasun	34	1986-10-19 7:00	25.02	Georgia
10	1977-11-13 12:00	43.75	Kim	35	2001-11-08 7:00	24.95	Lingling
11	1998-10-21 17:00	42.62	Babs	36	2008-06-21 11:00	23.65	Fengshen
12	1951-05-05 15:00	41.06	Iris	37	2011-07-26 12:00	23.45	Nock-Ten
13	1971-05-26 8:00	40.75	Dinah	38	1984-11-05 5:00	23.12	Agnes
14	1959-12-31 9:00	40.25	Harriet	39	1991-06-14 6:00	22.64	Yunya
15	1978-10-26 9:00	40.12	Rita	40	1962-05-18 0:00	22.61	Hope
16	1993-12-05 11:00	39.70	Lola	41	2007-11-27 15:00	22.55	Hagibis
17	1988-01-16 4:00	38.75	Roy	42	1994-10-20 22:00	21.92	Teresa
18	1967-11-03 19:00	38.53	Emma	43	2010-07-13 8:00	21.85	Conson
19	1952-10-21 16:00	38.14	Trix	44	2013-06-29 15:00	20.64	Rumbia
20	1983-07-14 16:00	37.63	Vera	45	1955-11-29 16:00	20.20	Patsy
21	1979-11-05 13:00	37.09	Vera	46	1992-10-26 6:00	19.90	Colleen
22	2015-12-14 15:00	36.01	Melor	47	1961-12-09 13:00	19.83	Ellen
23	1985-10-18 6:00	35.97	Dot	48	1956-12-09 10:00	19.60	Thelma
24	1989-10-10 18:00	35.30	Dan	49	2017-11-09 8:00	19.47	Haikui
25	1980-11-03 6:00	33.41	Betty	50	2005-11-10 7:00	17.40	Tembin

Among the 13 data kernels which represent the entire project coastline, there are several typhoons which appeared consistently in all annual maximum series of generated cyclonic wind speeds. Characteristics such as maximum sustained wind speed, minimum central pressure, and relative tracking of the top 50 typhoons are summarized in Table 3 below.

Table 3. Sample typhoon wind AMS at KP6 wind kernel.

Rank	Year / Int'l Name	V_{max} (kph)	P_c (hPa)	Track relative to the site	Closest distance to site (km)	Rank	Year / Int'l Name	V_{max} (kph)	P_c (hPa)	Track relative to the site	Closest distance to site (km)
1	1987 Betty	186.4	930.1	S	61.50	26	2004 Nina	174.0	940.0	N	140.88
2	1981 Irma	164.0	947.5	N	113.13	27	2000 Xangsane	118.6	976.8	N	19.09
3	2019 Kammuri	155.6	953.5	S	28.84	28	1960 Kit	134.3	967.6	S	56.79
4	2016 Nock-Ten	168.7	944.0	N	4.65	29	1982 Irving	102.6	985.1	S	37.66
5	1970 Joan	185.8	930.6	N	11.18	30	2003 Nepartak	91.7	990.1	S	174.63
6	1995 Angela	179.8	935.4	N	70.55	31	2012 Son-Tinh	75.9	996.3	S	190.19
7	2006 Durian	168.3	944.3	S	2.48	32	1966 Nancy	120.0	976.0	N	58.14
8	2014 Rammasun	167.4	945.0	N	6.09	33	2009 Nangka	82.0	994.1	S	99.53
9	2020 Goni	153.2	955.2	N	10.37	34	1986 Georgia	76.6	996.1	S	57.50
10	1977 Kim	186.6	930.0	N	125.91	35	2001 Lingling	85.7	992.6	S	245.83
11	1998 Babs	155.3	953.8	N	69.43	36	2008 Fengshen	143.1	962.0	S	143.32
12	1967 Emma	144.4	961.2	S	9.58	37	2011 Nock-Ten	87.6	991.8	N	92.59
13.5	1951 Iris	147.6	959.0	S	16.49	38	1984 Agnes	125.3	973.0	S	231.47
13.5	1971 Dinah	141.3	963.2	S	19.04	39	1991 Yunya	160.3	950.2	N	112.20
15	1978 Rita	218.9	901.9	N	109.31	40	1962 Hope	79.5	995.0	S	52.06
16	1993 Lola	145.4	960.5	N	80.74	41	2007 Hagibis	70.1	998.3	S	47.32
17	1959 Harriet	153.4	955.1	N	33.83	42	1994 Teresa	132.6	968.7	N	175.91
18	1988 Roy	120.6	975.7	S	32.72	43	2010 Conson	121.8	975.0	N	106.22

Table 3. Sample typhoon wind AMS at KP6 wind kernel.

Rank	Year / Int'l Name	V_{max} (kph)	P_c (hPa)	Track relative to the site	Closest distance to site (km)	Rank	Year / Int'l Name	V_{max} (kph)	P_c (hPa)	Track relative to the site	Closest distance to site (km)
19	1952 Trix	138.4	965.1	N	0.38	44	2013 Rumbia	58.0	1002.0	N	4.22
20	1979 Vera	182.7	933.2	N	140.16	45	1955 Patsy	70.8	998.1	S	10.66
21	1983 Vera	121.8	975.0	N	21.44	46	1956 Polly	105.4	983.7	N	75.41
22	2015 Melor	153.4	955.1	S	67.73	47	1961 Ellen	167.3	945.1	N	127.03
23	1985 Dot	192.8	924.9	N	126.97	48	1992 Colleen	112.6	980.0	N	180.31
24	1989 Dan	121.8	975.1	S	3.72	49	2017 Haikui	49.2	1004.3	S	28.64
25	1980 Belly	187.4	929.4	N	205.72	50	2005 Tembin	186.4	930.1	S	61.50

GENERATION OF TIDE PROPAGATION MODEL

A numerical model of the study area was developed using MIKE 21, which consists of a Hydrodynamic module (HD), and Spectral Wave module (SW). It can simulate the water level and current changes caused by various external forces. One of the primary forcings of the regional model is the time series of the astronomic tide level determined from a global tide forecast applied to the boundaries of the mesh; the time varying tide boundaries are allowed to propagate through the mesh and determine the tide levels and currents. The model also takes into consideration surface wind and pressure, which induce a shear stress on the water surface further driving the circulation.

An unstructured mesh was used to resolve the spatial scales required by the variation of depths and the irregular shape of the coastline. Two numerical domains were used for the analyses, namely the regional model encompassing the entire Philippine archipelago, and the local model limited to Ragay Gulf alone.

Regional Mesh

The bathymetric data used to develop the regional mesh was obtained from General Bathymetry Chart of the Oceans (GEBCO). GEBCO database provides gridded depth points at 30 arc-seconds, or approximately 1 km, intervals. The regional mesh (Fig. 7) becomes finer as it approaches the coastline of the Philippines to improve the accuracy of simulated hydrodynamics in this region.

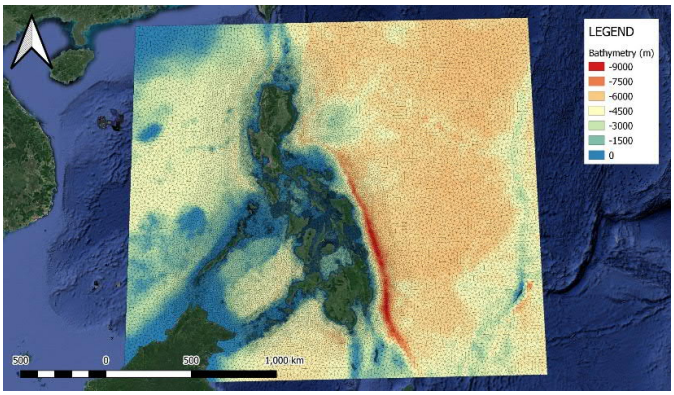

Figure 7. Domain extents for the hydrodynamic computation of the regional model.

From the results of the typhoon simulations for the regional model, hydrodynamic and wave parameters were extracted, which were then applied as boundary conditions to the HD and SW components of the local computation model. The hydrodynamic boundary conditions considered a flather condition which assigns both water surface elevation and current velocities at the boundaries of the domain, minimizing numerical instabilities at the boundaries compared to if only the tidal elevation was assigned (DHI, 2021). On the other hand, the spectral wave model's boundary conditions applied to the local domain included significant wave height, peak wave period, mean wave direction, and directional standard deviation for both wind-sea and swell wave components. The local typhoon simulations used a coupled hydrodynamic-spectral wave (HD-SW) model with two-way feedback on wave radiation (from SW model) and water levels (from HD model). The model parameters are the default settings of the model.

Local Mesh

All available bathymetric data was consolidated into a smaller unstructured local mesh (Fig. 8). This local mesh was created to ensure the fine changes in the coastline and detailed bathymetry can be properly reflected in the mesh; this contrasts with the regional mesh which has a relatively coarse grid that does not fully capture the local changes in bathymetry. It is this detailed nearshore bathymetry that will have a major effect on the behavior of the coastal inundation at the coastal areas.

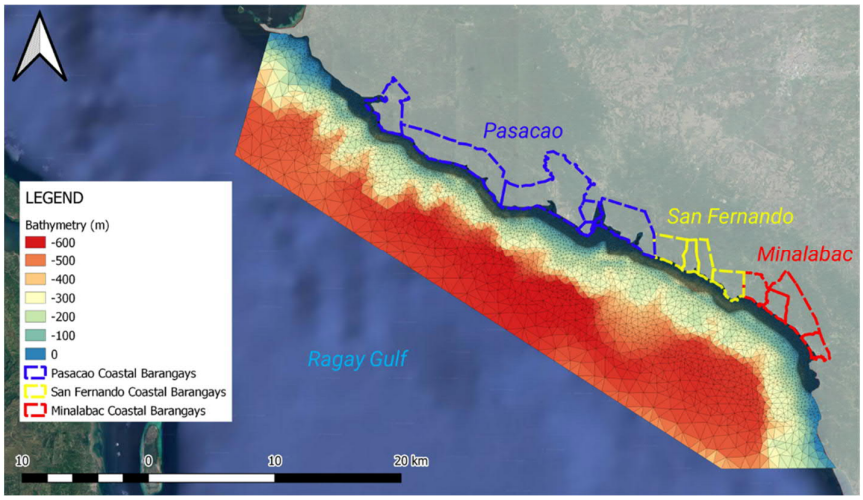

Figure 8. Local model extent.

SYNTHESIS OF COASTAL INUNDATION

Coastal inundation from the simulated 50 typhoons were analyzed through the extraction points along the project coastline (Fig. 9). These 70 points are located along the easement alignment, which ranges from 3m to 20m from the highest astronomical tide (HAT) towards the landward side.

Figure 9. Location of extraction points along the project coastline.

To illustrate the extent of storm tide inland, a coastal inundation envelope driven by the Top 30 typhoons (Table 3) in Brgy. Caranan, Pasacao is shown in Figure 10. It is seen that the coastal inundation along the shore is up to 3m and the reached as far as 650 m from the shoreline, as the presence of Caranan River allows the entry of water from the sea towards the low-lying areas at the flood plains of the river.

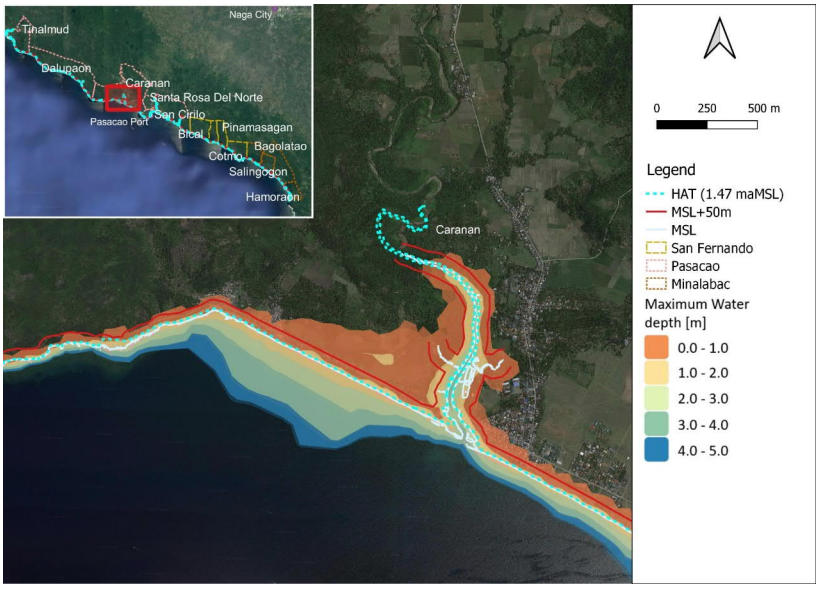

Figure 10. Inundation envelope of 30 simulated typhoons in Brgy. Caranan, Pasacao.

Annual Maximum Series of Coastal Inundation

AMS of coastal inundation was extracted for each extraction point. Table 4 below shows a sample AMS for point PT-1 located in Brgy. Tinalmud, Municipality of Pasacao.

Table 4. AMS of coastal inundation at PT-1.

Year	Coastal Inundation (m)	Year	Coastal Inundation (m)	Year	Coastal Inundation (m)
1951	0.61	1982	1.01	2004	0.58
1952	1.53	1983	0.81	2005	0.74
1955	0.73	1984	0.74	2006	1.04
1956	0.57	1985	0.36	2007	0.39
1959	1.08	1986	0.50	2008	0.61
1960	0.57	1987	0.73	2009	0.50
1961	0.71	1988	1.27	2010	0.81
1962	0.73	1989	0.64	2011	0.34
1966	1.03	1991	0.94	2012	0.72
1967	0.75	1992	0.58	2013	0.57
1970	0.61	1993	1.25	2014	0.72
1971	0.79	1994	0.59	2015	0.91
1977	1.61	1995	0.99	2016	0.52
1978	0.48	1998	0.78	2017	0.65
1979	0.91	2000	0.81	2019	1.01
1980	0.59	2001	0.75	2020	0.73
1981	0.72	2003	0.60		

Extreme Value Analysis

Extreme Value Analysis (EVA) is a known statistical tool in analyzing a dataset of a subject parameter. In this analysis, the probability of an extreme event occurring is estimated using the maximum values of a dataset of the subject parameter. This type of analysis is best in identifying risks because it characterizes the behavior of the tails of a larger distribution, which is heavily influenced by the outliers or the extremes. It is best suited for modeling low probability, high impact events such as coastal flooding induced by high storm tide levels.

The EVA tool of MIKE 21 was used to determine the best-fit probability distribution and subsequently the coastal inundation of specified return periods along the project coastline. Eight (8) probability distributions were used - Generalized Extreme Value (GEV), Gumbel (GUM), Weibull (WEI), Gamma/Pearson Type 3 (P3), Log-Pearson Type 3 (LP3), Log-normal (LN2), Generalized Pareto (GP), and Fréchet (FRE). The parameters of these probability distribution models were estimated by Method of Moments. These distributions were evaluated against the AMS of STL for each point and tested using the Kolmogorov-Smirnov (K-S) parameter (Table 5).

Table 5. Probability density functions and their corresponding K-S parameter for each extraction point.

Legend		Lowest K-S and best-fit visually on higher RPs			Lowest K-S but not best-fit visually on higher RPs		Not lowest K-S but best-fit visually on higher RPs		
Barangay	**Point**	**K-S for each probability distributions**							
		GEV	**GUM**	**WEI**	**P3**	**LP3**	**LN2**	**GP**	**FRE**
Tinalmud	PT-1	0.10	0.12	0.12	0.12	0.11	0.15	0.14	0.09
	PT-2	0.13	0.13	0.17	0.17	0.13	0.13	0.18	0.12
	PT-3	0.10	0.12	0.09	0.09	0.08	0.15	0.11	0.08
	PT-4	0.13	0.13	0.17	0.17	0.13	0.14	0.18	0.13
Dalupaon	PD-1	0.16	0.15	0.21	0.21	0.16	0.16	0.21	0.15
	PD-2	0.16	0.15	0.21	0.21	0.15	0.14	0.21	0.15
	PD-3	0.13	0.13	0.16	0.15	0.13	0.13	0.18	0.13
	PD-4	0.16	0.15	0.21	0.21	0.15	0.14	0.21	0.15
	PD-5	0.16	0.18	0.22	0.22	0.17	0.19	0.21	0.16
	PD-6	0.13	0.14	0.16	0.15	0.13	0.13	0.19	0.14
	PD-7	0.16	0.15	0.20	0.19	0.14	0.13	0.21	0.16
	PD-8	0.14	0.14	0.19	0.18	0.14	0.15	0.19	0.14
	PD-9	0.14	0.15	0.18	0.18	0.15	0.17	0.19	0.13
	PD-10	0.14	0.14	0.19	0.19	0.15	0.15	0.19	0.13
	PD-11	0.14	0.14	0.19	0.19	0.14	0.14	0.20	0.14
	PD-12	0.19	0.18	0.24	0.29	0.19	0.15	0.23	0.14
Caranan	PC-1	0.13	0.14	0.12	0.12	0.10	0.14	0.15	0.08
	PC-2	0.11	0.12	0.11	0.11	0.10	0.15	0.13	0.09
	PC-3	0.09	0.10	0.09	0.08	0.07	0.13	0.10	0.09
	PC-4	0.12	0.13	0.08	0.09	0.10	0.16	0.09	0.12
	PC-5	0.11	0.12	0.08	0.08	0.08	0.15	0.10	0.11
	PC-6	0.14	0.15	0.16	0.17	0.15	0.16	0.18	0.11
	PC-7	0.13	0.14	0.15	0.16	0.14	0.15	0.17	0.10
	PC-8	0.11	0.12	0.10	0.10	0.10	0.14	0.13	0.08
	PC-9	0.11	0.13	0.11	0.11	0.10	0.13	0.14	0.08
Santa Rosa Del Sur	PSR-1	0.12	0.13	0.13	0.13	0.12	0.15	0.15	0.09
	PSR-2	0.12	0.13	0.16	0.15	0.13	0.16	0.17	0.11
	PSR-3	0.15	0.14	0.19	0.19	0.15	0.15	0.20	0.14
	PSR-4	0.16	0.16	0.21	0.22	0.17	0.18	0.21	0.15
	PSR-5	0.14	0.14	0.17	0.16	0.14	0.14	0.19	0.14
	PSR-6	0.10	0.10	0.13	0.12	0.10	0.11	0.15	0.10
San Cirilo	PSC-1	0.09	0.10	0.11	0.10	0.09	0.12	0.12	0.07
	PSC-2	0.09	0.10	0.11	0.11	0.09	0.11	0.12	0.07
Balogo	PB-1	0.09	0.09	0.10	0.10	0.08	0.12	0.12	0.07
	PB-2	0.09	0.10	0.09	0.09	0.08	0.13	0.11	0.06
	PB-3	0.10	0.11	0.10	0.10	0.09	0.14	0.12	0.08
	PB-4	0.11	0.11	0.10	0.10	0.09	0.15	0.12	0.09
	PB-5	0.12	0.12	0.15	0.14	0.12	0.13	0.16	0.11
	PB-6	0.09	0.10	0.10	0.10	0.09	0.13	0.12	0.07
	PB-7	0.12	0.12	0.16	0.15	0.13	0.14	0.17	0.12
	PB-8	0.14	0.14	0.18	0.17	0.14	0.14	0.19	0.14
	PB-9	0.14	0.14	0.17	0.16	0.13	0.13	0.19	0.14
Bical	SFB-1	0.13	0.13	0.16	0.15	0.13	0.13	0.18	0.13
	SFB-2	0.16	0.16	0.22	0.23	0.17	0.17	0.21	0.15
	SFB-3	0.16	0.16	0.22	0.22	0.16	0.13	0.21	0.16
	SFB-4	0.14	0.14	0.17	0.16	0.13	0.13	0.19	0.14
Gñaran	SFG-1	0.14	0.15	0.17	0.18	0.15	0.17	0.19	0.12
	SFG-2	0.12	0.11	0.14	0.13	0.12	0.13	0.16	0.11
Pinamasagan	SFP-1	0.08	0.08	0.10	0.09	0.08	0.11	0.12	0.07
	SFP-2	0.13	0.14	0.13	0.13	0.12	0.16	0.16	0.10

Table 5. Probability density functions and their corresponding K-S parameter for each extraction point.

Legend		Lowest K-S and best-fit visually on higher RPs			Lowest K-S but not best-fit visually on higher RPs			Not lowest K-S but best-fit visually on higher RPs	
Barangay	**Point**	**K-S for each probability distributions**							
		GEV	**GUM**	**WEI**	**P3**	**LP3**	**LN2**	**GP**	**FRE**
	SFP-3	0.14	0.14	0.18	0.17	0.15	0.15	0.19	0.13
Cotmo	SFC-1	0.14	0.14	0.18	0.17	0.15	0.16	0.19	0.13
	SFC-2	0.14	0.14	0.17	0.18	0.15	0.16	0.18	0.12
	SFC-3	0.13	0.10	0.10	0.09	0.16	0.11	0.10	0.09
	SFC-4	0.13	0.11	0.11	0.10	0.16	0.12	0.11	0.10
	SFC-5	0.11	0.12	0.10	0.09	0.08	0.15	0.11	0.09
	SFC-6	0.17	0.17	0.22	0.23	0.16	0.14	0.22	0.16
	SFC-7	0.17	0.17	0.21	0.21	0.17	0.15	0.22	0.16
Bagolatao	MB-1	0.15	0.15	0.20	0.20	0.16	0.16	0.20	0.15
	MB-2	0.15	0.15	0.20	0.19	0.14	0.13	0.20	0.15
	MB-3	0.17	0.17	0.23	0.24	0.17	0.14	0.22	0.17
San Antonio	MSA-1	0.14	0.14	0.11	0.13	0.13	0.17	0.13	0.14
	MSA-2	0.18	0.18	0.24	0.26	0.19	0.16	0.23	0.16
Salingogon	MS-1	0.12	0.13	0.12	0.12	0.11	0.16	0.14	0.10
	MS-2	0.12	0.12	0.10	0.09	0.09	0.15	0.11	0.11
	MS-3	0.08	0.09	0.08	0.08	0.07	0.11	0.09	0.08
Hamoraon	MH-1	0.11	0.11	0.08	0.08	0.08	0.14	0.09	0.10
	MH-2	0.10	0.11	0.08	0.08	0.08	0.14	0.10	0.09
	MH-3	0.09	0.09	0.07	0.06	0.07	0.11	0.09	0.08
	MH-4	0.11	0.11	0.10	0.10	0.09	0.14	0.12	0.09

Since the K-S value does not vary significantly across the distributions, visual inspection was done such that the extremes are close to the curve. This is in consideration that the 100-yr return period is the basis of design for urban areas (DPWH DGCS Volume 3, 2015), which is the prominent land use along the project coastline. For rural/agricultural areas, 25-yr is the prescribed return period. To illustrate, a sample probability plot for PT-1 is shown in Figure 11. Fréchet distribution inclines closer to the extreme values relative to the other distributions so it was deemed to be best fit to represent the STL AMS.

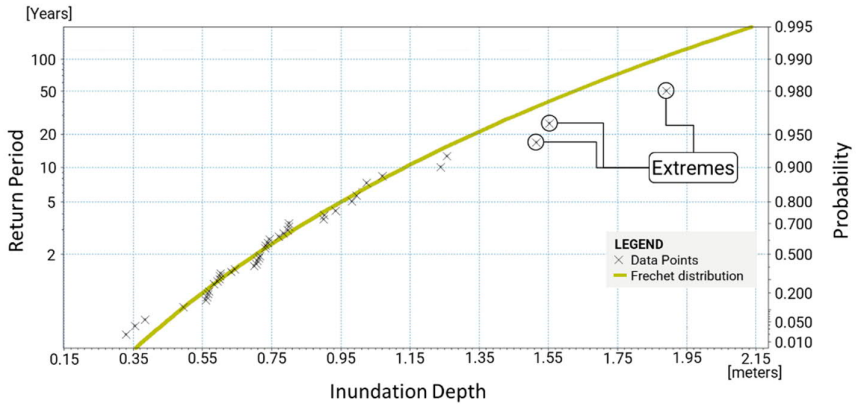

Figure 11. Sample probability plot showing the best distribution considered (at PT-1).

Upon generating the best-fit probability distribution for each extraction point, the coastal inundation corresponding to various return periods are summarized as shown below in Table 6.

Table 6. Corresponding coastal inundation of 10-yr, 25-yr, 30-yr, 75-yr, and 100-yr return periods.

Barangay	Point	Land Use	Return Period					
			10-yr	**25-yr**	**30-yr**	**50-yr**	**75-yr**	**100-yr**
Tinalmud	PT-1	U	1.16	1.42	1.46	1.64	1.77	1.88
	PT-2	U				0.12	0.29	0.38

Table 6. Corresponding coastal inundation of 10-yr, 25-yr, 30-yr, 75-yr, and 100-yr return periods.

Barangay	Point	Land Use	Return Period					
			10-yr	25-yr	30-yr	50-yr	75-yr	100-yr
	PT-3	U	0.38	0.71	0.75	0.92	1.1	1.19
	PT-4	U		0.23	0.28	0.38	0.59	0.7
Dalupaon	PD-1	U	0.35	0.71	0.76	1.01	1.16	1.34
	PD-2	U				0.11	0.28	0.4
	PD-3	U	0.59	0.85	0.89	1.03	1.15	1.23
	PD-4	A		0.1	0.14	0.32	0.49	0.6
	PD-5	A		0.09	0.14	0.39	0.6	0.74
	PD-6	U	1.58	1.82	1.84	1.97	2.08	2.14
	PD-7	U	0.04	0.3	0.34	0.5	0.62	0.72
	PD-8	U	0.38	0.68	0.73	0.91	1.06	1.18
	PD-9	A		0.33	0.38	0.58	0.76	0.88
	PD-10	U	0.47	0.83	0.86	1.12	1.31	1.43
	PD-11	A	0.12	0.43	0.47	0.66	0.82	0.93
	PD-12	A						0.1
Caranan	PC-1	A		0.22	0.28	0.55	0.77	0.94
	PC-2	U	0.37	0.71	0.75	0.96	1.13	1.25
	PC-3	U		0.12	0.17	0.38	0.54	0.66
	PC-4	A	0.29	0.63	0.68	0.89	1.05	1.18
	PC-5	A	0.28	0.66	0.72	0.94	1.12	1.25
	PC-6	U	0.52	0.92	0.98	1.21	1.44	1.57
	PC-7	U	0.37	0.72	0.77	0.98	1.17	1.28
	PC-8	U	0.31	0.62	0.67	0.84	1	1.09
	PC-9	U	0.43	0.78	0.82	1.02	1.2	1.31
Santa Rosa Del Sur	PSR-1	U	0.05	0.39	0.43	0.62	0.78	0.88
	PSR-2	U		0.23	0.27	0.49	0.65	0.77
	PSR-3	U		0.22	0.27	0.47	0.65	0.76
	PSR-4	U	0.15	0.58	0.63	0.88	1.1	1.24
	PSR-5	U	0.65	0.92	0.96	1.13	1.26	1.35
	PSR-6	U	1.01	1.27	1.31	1.47	1.58	1.67
San Cirilo	PSC-1	U	0.61	0.95	1	1.2	1.36	1.47
	PSC-2	U	1.54	1.84	1.88	2.08	2.22	2.34
Balogo	PB-1	U	0.78	1.09	1.13	1.32	1.47	1.57
	PB-2	U	0.24	0.58	0.6	0.82	0.98	1.1
	PB-3	U	0.4	0.73	0.77	0.97	1.12	1.23
	PB-4	U	0.72	1.02	1.05	1.23	1.36	1.47
	PB-5	U	0.63	0.89	0.92	1.07	1.18	1.26
	PB-6	U	0.5	0.8	0.84	1.02	1.15	1.25
	PB-7	A	1.27	1.53	1.55	1.71	1.83	1.91
	PB-8	A	0.81	1.07	1.09	1.29	1.41	1.51
	PB-9	A	1.28	1.58	1.62	1.78	1.91	2
Bical	SFB-1	U	1.02	1.29	1.32	1.48	1.6	1.68
	SFB-2	U	0.18	0.51	0.56	0.74	0.9	1.01
	SFB-3	U	0.11	0.52	0.58	0.81	1.01	1.14
	SFB-4	U	0.96	1.26	1.29	1.46	1.59	1.68
Gñaran	SFG-1	U	0.49	0.93	0.99	1.26	1.48	1.65
	SFG-2	U	0.95	1.18	1.21	1.34	1.44	1.51
Pinamasagan	SFP-1	U	1.42	1.67	1.7	1.84	1.94	2.02
	SFP-2	U	0.75	1.09	1.14	1.34	1.51	1.62
	SFP-3	U	0.26	0.61	0.66	0.86	1.03	1.15
Cotmo	SFC-1	U	0.48	0.82	0.85	1.04	1.18	1.29
	SFC-2	U	0.15	0.49	0.55	0.74	0.91	1.03
	SFC-3	U	1.05	1.4	1.45	1.65	1.82	1.95
	SFC-4	U	0.54	0.88	0.92	1.1	1.28	1.4
	SFC-5	U		0.32	0.37	0.58	0.76	0.89
	SFC-6	U	0.11	0.42	0.46	0.65	0.81	0.91
	SFC-7	U	1.05	1.39	1.43	1.63	1.79	1.91
Bagolatao	MB-1	U	0.95	1.24	1.27	1.44	1.58	1.68
	MB-2	U	0.46	0.84	0.89	1.11	1.31	1.44
	MB-3	U	0.74	1.07	1.11	1.3	1.48	1.6
San Antonio	MSA-1	A	1.4	1.65	1.68	1.82	1.92	2
	MSA-2	U			0.04	0.26	0.46	0.61
Salingogon	MS-1	U	0.17	0.51	0.56	0.76	0.92	1.04

Table 6. Corresponding coastal inundation of 10-yr, 25-yr, 30-yr, 75-yr, and 100-yr return periods.

Barangay	Point	Land Use	Return Period					
			10-yr	25-yr	30-yr	50-yr	75-yr	100-yr
	MS-2	U	0.63	1.15	1.19	1.37	1.51	1.62
	MS-3	U	0.25	0.67	0.91	0.87	1.01	1.11
Hamoraon	MH-1	U	0.41	0.74	0.78	0.96	1.11	1.22
	MH-2	U	0.42	0.74	0.78	0.96	1.11	1.22
	MH-3	U	0.48	0.8	0.84	1.02	1.17	1.27
	MH-4	U	0.53	0.86	0.9	1.1	1.25	1.35

* U – urban, A – agricultural/rural

CONCLUSIONS

Based on the data, engineering analyses, and syntheses of numerical simulation results for the study area, the following are found out:

1. There were 102 shortlisted potentially critical cyclones from 1951 to 2020 that were deemed to induce the maximum cyclonic wind speed along the project shoreline. These were further trimmed down to 50 based on AMS of kernel winds in the site, reducing the number of cyclones to be analyzed significantly.
2. Higher wind speed in the site did not necessarily produce the higher coastal inundation. As seen in Table 4, 1977 Typhoon Kim and 1952 Typhoon Trix induced the top 2 highest coastal inundation at PT-1 despite ranking 10th and 19th, respectively, in terms of wind speed experienced in the site. There are other factors that affect storm tide such as wind pressure and track of the typhoon relative to the site. Numerical simulations are suggested to quantify the consolidated effects of these parameters.
3. Based on statistical analysis performed in this study, a significant number of cases where the probability distribution was chosen purely based on visual inspection of the plot such that it should be leaning closest to the extremes, albeit the K-S parameter suggests a better fit. It is advised to investigate additional goodness-of-fit tests to quantitatively determine the probability distribution that most accurately represents the extremes.
4. From the resulting EVA of coastal inundation, the corresponding coastal inundation of specified return periods for design were determined. For rural/agricultural areas with 25-yr level of protection required, coastal inundation reaches up to 1.65 m while for urban areas with 100-yr level of protection required, coastal inundation ranges from 0.38 to 2.34 m. Coastal protection structures to be proposed should be designed higher than these design water levels and account in addition for anticipated wave run-up along the face of proposed structures and freeboard of 0.6 m as per DPWH DGCS Volume 3 (2015). After the acceptable-risk level of the seawall design is determined, the horizontal alignment of contemplated seawall segments can be designed. Figure 12 shows one preliminary segment of a gravity-type seawall in Pasacao municipality, showing the plan alignment and shoreline setback from the highest astronomic tide (HAT) conforming to the Water Code, as well as the typical geometry and proportions of a seawall section.

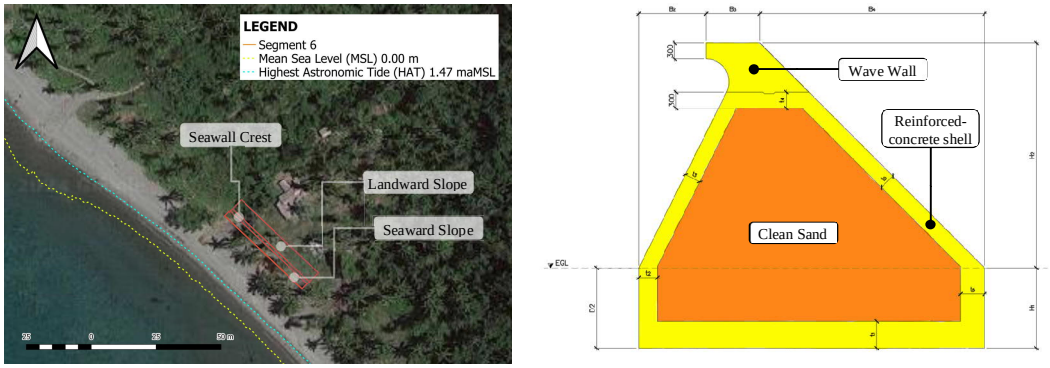

Figure 12. Plan alignment of Segment 6 and typical section of gravity-type seawall.

ACKNOWLEDGEMENT

This paper is an outcome of a collaborative engineering research project between the UP National Engineering Center and the DPWH Flood Control and Sabo Engineering Center (FCSEC). The project focuses on pre-development and post-development coastal engineering studies for seawall segments along three municipal coastlines in Camarines Sur.

REFERENCES

Camelo, J.B., Cruz, E.C., and Cruz, L.L.B. (2017). Simulative analysis of inland inundation behind Roxas Boulevard seawall due to storm tide overtopping by historical typhoons. Proceedings, 9th International Conference on Asian and Pacific Coasts (APAC 2017), SBN 978-981-3233-80-5, pp. 235-246

Cruz, E.C., Santos, J.C.E.L., Camelo, J.B., Zarco, M.H., del Rosario M.E.L., Gargullo, J.M.B., Inocencio, I.A.D., and Cruz, L.L.B. (2016) Preliminary engineering of a seawall against storm tides and waves along a built-up waterfront. Proceedings, 26th (2016) International Ocean and Polar Engineering Conference (ISOPE) Rhodes, Greece, ISBN 978-1-880653-88-3; ISSN 1098-6189. 1428-1435

Department of Public Works and Highways. (2015). Design Guidelines, Criteria and Standards (DGCS) Volume 3: Water Engineering Projects.

Department of Public Works and Highways. (2018). Terms of Reference – Consulting Services for the Feasibility Study and Detailed Engineering Design for the Proposed Seawall Alignment in the Municipalities of Minalabac, Pasacao, and San Fernando, Camarines Sur. Philippines.

DHI. (2019). Mike 21 Extreme Value Analysis User Guide.

DHI. (2021). Mike 21 Flow Model Hydrodynamic Module User Guide.

DHI. (2022). Global Tide Model Data. Retrieved from DHI MIke21 Online Documentation: http://doc.mikepoweredbydhi.help/webhelp/2021/TidePredictionHeights/TidePredictionHeights/TidePredictionHeightsDialog/Global_Tide_Model_Data.htm#XREF_78009_18_3_Global_Time

Holland, G. (1980). An analytical model of the wind and pressure profiles in hurricanes. Monthly weather review, Volume 108, pp.1212-1218.

IHO & IOC. (2022). GEBCO's Global Gridded Bathymetric Data Set. International Hydrographic Organization & Intergovernmental Oceanographic Commission.

National Oceanic and Atmospheric Administration. (2019). Storm Surge Overview. National Hurricane Center and Central Pacific Hurricane Center. https://www.nhc.noaa.gov/surge/

Rizabal, K.D.S. and Cruz, E.C. (2020) Hydrodynamic analysis of Leyte Tide Embankment against coastal flooding due to Typhoon Haiyan 2013. Proceedings, PICE Virtual National Convention and Technical Conference, 20-21 November 2020.